FeS@rGO nanocomposites as electrocatalysts for enhanced chromium removal and clean energy generation by microbial fuel cell

Jafar Ali [a, b], Lei Wang *, [a], Hassan Waseem [c], Gang Pan *, [a b, d]

A Key Laboratory of Environmental Nanotechnology and Health Effects, Research Center for Eco-environmental Sciences, Chinese Academy of Sciences, 18 Shuangqing Road, Beijing 100085, P. R. China.

[b] *University of Chinese Academy of Sciences, Beijing 100049, P. R. China*

[c] *Department of Environmental Engineering, Michigan State University, East Lansing, MI 48823, USA*

[d] *Centre of Integrated Water-Energy-Food Studies, School of Animal, Rural and Environmental Sciences, Nottingham Trent University, Brackenhurst Campus, Southwell NG25 0QF, United Kingdom*

* Corresponding author: leiwang@rcees.ac.cn (L. Wang); gpan@rcees.ac.cn (G. Pan)

Abstract

Bioelectrochemical removal of Cr(VI) and consequent renewable energy generation from wastewater is a promising technology. However, slow reaction kinetics, expensive catalysts, and hydrophobic binders remain a significant challenge for commercialization of this emerging technology. In the present study, for the first time graphite felt modified with FeS@rGO nanocomposites were used as a cathode in a dual chamber microbial fuel cell (MFC) for concurrent Cr(VI) reduction and power generation. The MFC with FeS@rGO nanocomposites (MFC-FeS@rGO) exhibited 100% Cr(VI) removal efficiency for the concentration of 15 mg/L and also acquired high reduction rate of 1.43 mg/L/h, which was approximately 4.6 times higher than MFC-blank. MFC-FeS@rGO delivered the maximum power density of 90.4 mW/m^2, and it was 150% high as that of MFC-blank (36 mW/m^2). High cathodic coulombic efficiency for MFC-FeS@rGO (61%) indicated the substantial amount of

charge produced by exoelectrogens was consumed for Cr(VI) reduction. Overall improved electrochemical performance of MFC-FeS@rGO was attributed to the high conductivity, low internal resistance, and better reaction kinetics of FeS@rGO nanocomposites. This study has demonstrated the highest reduction rate and high power production compared with previous studies which have used very high concentration of Cr(VI). Hence, it is expected that current findings will help to scale up the simultaneous Cr(VI) reduction and power generation from real wastewater.

Keywords: Electrochemical; Microbial fuel cell; Chromium; Renewable energy; Wastewater treatment

1. Introduction

The presence of chromium in the aquatic environment poses a severe threat to human health and ecosystem due to non-degradability and high toxicity. Long-term exposure of Cr(VI) to human beings can cause dermatitis, tumours, liver and kidney damage, bronchogenic, and respiratory problems [1]. Cr(VI), owing to its high toxicity, has been classified as a class-I carcinogen by the International Agency Research on Cancer and U.S. Environmental Protection Agency (EPA) has declared 50 μg/L of Cr(VI) as a permissible limit in drinking water [2, 3]. The release of Cr(VI) into the aquatic environment is mainly through wastewater effluents of electroplating, metallurgy, leather tanning, and dyes manufacturing industries [4]. On the other hand, Cr(III) is more stable and less toxic than Cr(VI), which is relatively more corrosive, water-soluble, and mobile [5]. Therefore, the reduction/ transformation of Cr(VI) into Cr(III) is necessary before the discharge of industrial effluents in the environment. Current approaches for the reduction of Cr(VI) include solvent extraction, bioaccumulation, reverse osmosis, photoelectrochemical process, ion exchange, adsorption, and electrochemical precipitation [6-8].

However, the practices mentioned above are less effective due to the high energy requirements, expensive and laborious nature, and excessive sludge production. Microbial fuel cell (MFC) mediated reduction of Cr(VI) holds great promise due to renewable energy, low cost, and high sustainability[9, 10]. Though substantial reduction rates of Cr(VI) have been achieved by MFC, slow reduction kinetics remains a significant bottleneck [10, 11]. In literature, usually high concentration (100-200 mg/L) of Cr(VI) has been reportedly used to show the high removal efficiency with high power production by MFC. The high concentration of Cr(VI) is unrealistic and is far from practical applications. Furthermore, electrical repulsion between electronegative species of Cr ($Cr_2O_7^{2-}$ or CrO_4^-) and negatively charged cathode can

slow down the reaction kinetics. Passivation of Cr(III) on the cathode surface can also lower the conductivity [11]. Besides, biocathode toxicity is the major drawback of biological reduction of Cr(VI) [12]. Thus, electrode modifications through efficient catalytic materials are required for accelerated reduction of Cr(VI) in real wastewater.

Iron-based materials such as pyrite, magnetite, and mackinawite have been frequently used for catalysing the Cr(VI) reduction from the wastewater and sediments [13-15]. However, a few studies are available which have targeted the Cr(VI) reduction by iron-based materials in MFCs. For example, Shi, Zhao, Liu, Jiang and Ding [16] employed the natural pyrrhotite-coated cathode for understanding the Cr(VI) reduction under various conditions. In another study, Fe(III) was used as an electron-shuttle for enhanced Cr(VI) reduction in MFC by minimizing the diffusional resistance and overpotential [11]. Recently, α-Fe_2O_3/polyaniline nanocomposites were evaluated to catalyse performance of Cr(VI) reducing MFC [10]. Unfortunately, studies mentioned above still have some drawbacks such as very high concentration of Cr(VI), slow reaction kinetics, passivation of Cr(III) and low power production which limit their practical applications. Electrochemical reduction of Cr(VI) is limited by Fe (0) and Fe (II)-bearing oxides under neutral to basic pH.

Nonconductive and expensive binders could reduce the conductivity and block the active sites to reduce permeability at the electrode-electrolyte interface [17]. Poor durability of costly materials and harmful impacts due to their dissolution over time may limit these strategies for long term applications. Besides, externally added mediators might not be a cost-effective and sustainable approach at all [11]. Thus, more efficient iron-based catalyst and less expensive binders with superior hydrophilic properties can be employed to enhance the reduction of Cr(VI) in MFC for practical applications. Intriguingly, FeS nanoparticles have been widely used in various fields like photo-catalysis and sodium and lithium-ion batteries due to low cost and eco-friendly nature [18, 19].A recent study has proposed that FeS nanoparticles can facilitate extracellular electron transport in MFC [20]. Hydrophilic conductive binders (BPSH-40) and graphene could be a better choice in cathode catalysts development to reduce the precipitation of Cr(III) and low conductivity [17]. There has also been an upsurge in the knowledge of graphene-based materials and their applications in electrochemistry due to excellent conductivity, large surface area, and good mechanical strength [21]. Inspired from the above studies, we propose FeS nanomaterials decorated with reduced graphene oxide (FeS@rGO) could be an ideal cathode modifier for simultaneously enhanced Cr(VI) reduction and electricity production in MFC. To the best of our knowledge, the utility of this material has not been evaluated for Cr(VI) reduction and power deneration

by MFCs. Herein we report that cathode decorated with FeS@rGO nanocomposites can accelerate the Cr(VI) reduction in MFC. The enhanced bioelectrochemical reduction was attributed to the high conductivity and active catalytic surface of FeS@rGO. Detailed reduction kinetics and improved cathodic coulombic efficiency suggested that current findings could help to scale up the simultaneous Cr(VI) reduction and power generation from real wastewater.

2. Materials and methods

2.1. Electrolyte preparation and anodic inoculum

Annolyte was prepared by dissolving the (g/L) 4.4 KH_2PO_4, 3.4 K_2HPO_4, 1.0 KNO_3, 0.5 NaCl, 0.2 $MgSO_4$, $CaCl_2$ 0.014 of distal water. One mL from trace elements media containing the (mg/L) 0.39 $Na_2MoO_4 \cdot 2H_2O$, 0.22 $ZnSO_4 \cdot 7H_2O$, 1.81 $MnCl_2 \cdot 4H_2O$, 0.08 $CuSO_4 \cdot 5H_2O$, and 2.86 H_3BO_3 was supplemented in the above solution. However, catholyte contained, (g/L) 0.31 NH_4Cl, 0.13 KCl, 4.97 NaH_2PO_4, 2.75 Na_2HPO_4, and 15 mg/L of hexavalent chromium. The pH of catholyte was adjusted to 2.0 using 0.1 M HCl solution. Anodic effluent from the previously working MFC was used as an anodic inoculum source.

2.2. FeS@rGO *nanocomposite synthesis and characterization*

Fabrication of FeS wrapped reduced graphene (FeS@rGO) nanocomposites was carried out by a slightly modified method described elsewhere in the literature [18]. Briefly, graphene oxide suspension in DI (6 mg/mL) was prepared by sonication to disperse the GO nanosheets thoroughly. For the typical fabrication of FeS@rGO 4.0 g of iron nitrate [$Fe(NO_3)_3 \cdot 9H_2O$] was dissolved in 40 mL of deionized water, and 12 mL of GO suspension was mixed under vigorous stirring and sonicated for one h. Subsequently, dropwise adding the freshly prepared sodium sulfide nonahydrate ($Na_2S \cdot 9H_2O$) solution (3.6 g in 20 mL) under vigorous stirring. Black precipitate appeared immediately, and the mixture was stirred and sonicated each for 1h (Fig.1). Finally, the precipitate was collected by centrifugation and washed thrice with the deionized water. Vacuum incubator was used to dry the precipitate which was then transferred to a quartz tube furnace and annealed at 400 °C in a nitrogen atmosphere for 2 h to reduce GO and increase the FeS crystallinity.

However, FeS without GO was also prepared under the similar condition to be used as a control. The structural morphology of nanocomposites was characterized by scanning electron microscopy (SEM, S4800, HITACHI) and HR-TEM (JEM-2100 plus transmission electron microscope, JEOL, Tokyo, Japan). Chemical and structural characterization was done by X-ray diffraction analysis (XRD, PANalytical Empyrean, diffractometer equipped with a

Cu Kα1 radiation) and Fourier transform infrared spectroscopy (FTIR 200-VT, Perkin-Elmer, Shelton, CT). The elemental composition and chemical state of nanocomposites were analysed by X-ray photoelectron spectroscopy (XPS, ESCALAB-250).
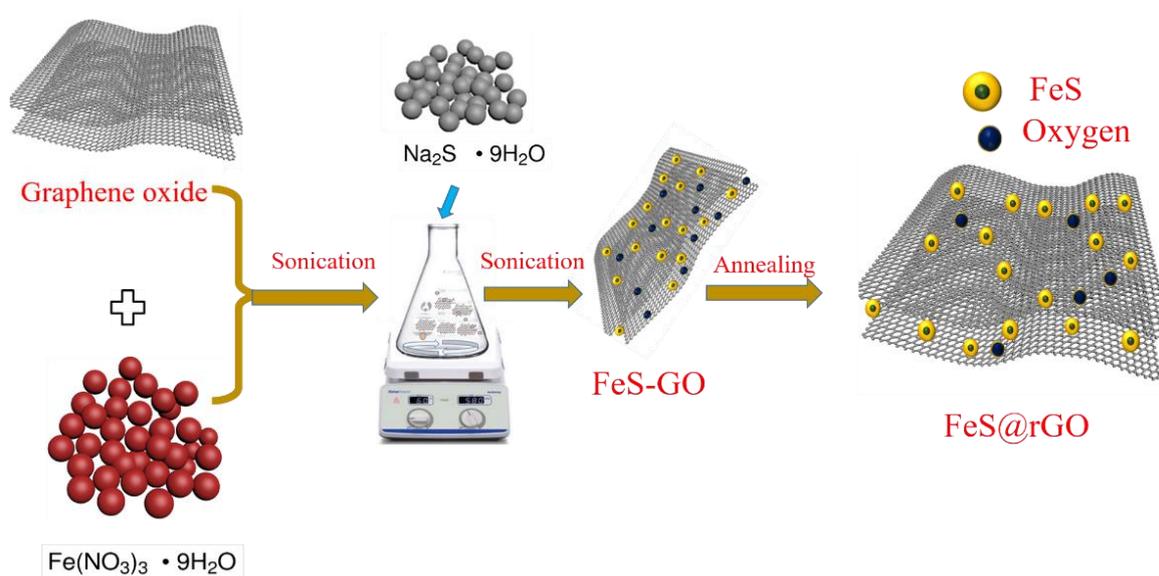
Fig. 1. Schematic illustration of the facile synthesis of FeS wrapped reduced graphene (FeS@rGO) nanocomposites

2.3. Electrode construction

Graphite felt (4 × 2.5 cm) was purchased from Shanghai Hesen Electrical Co., Ltd. and used in anode and cathode materials. Pre-treatment of electrodes was done by overnight incubation in acetone solution followed by heating in a muffle furnace at 450 °C about 30 min as already described in the literature [22, 23]. Catalytic ink was prepared using the 5 mg/cm^2 of FeS@rGO nanocomposites into a mixture containing a hydrophilic binder (BPSH-40) and N, N- dimethylformamide followed by ultrasonication as described previously [17]. Subsequently, the cathode was decorated in such a way that a uniform catalyst layer was coated on graphite felt. Similarly, one control electrode was also prepared with FeS nanocomposites, and one blank electrode was used without any modification. Modified cathodes were dried in the incubator at 60 °C for 24 h and kept for further use. However, anode was used without any modification after pre-treatment.

2.3. MFC construction and operation

In this study, three identical dual chamber microbial fuel cells (MFCs) made of Plexiglass were designed. Each chamber had an effective working volume of 140 mL. MFCs

were named with respect to the cathode modified material e.g., MFC-FeS@rGO, MFC-FeS, and MFC-blank (without any modification). Proton exchange membrane (PEM, Nafion™ 117, Dupont Co.) with an active surface area 12.56 cm^2 was used to separate the anode and cathode. Pre-treatment of PEM was done by consecutively boiling it in H_2O_2 (30% v/v) and H_2SO_4 (0.5 M), each for 1 h and then stored in deionized water until further use. After MFC construction annolyte and catholyte were filled in respective chambers. Nitrogen purging was performed to remove dissolved oxygen from each chamber. Annolyte from another MFC reactor was used as anodic inoculum. The distance between two electrodes was 4 cm, and the copper wire was used to connect the electrodes via external load (1000 Ω). All MFCs were incubated at room temperature and allowed to run in open circuit mode. When a stable open circuit potential was achieved, the MFCs were ready for electrochemical analysis. Annolyte and catholyte were replaced from time to time when open circuit potential (OCP) was below the 0.3 V.

2.4. Electrochemical characterization and calculations

Electrochemical characterization was started with the polarization curves drawn by varying the external resistance (1000, 700, 500, 300, 100 to 50 Ω) at 20 min intervals after the stabilized OCP was obtained. The potential drop across the external resistance was recorded for 20 min interval by digital multimeter data acquisition system (M2700, Keithley instrument, Cleveland, USA) connected with the computer. Ohms law was used to calculate current and power from voltage data as (V= IR$_{ext}$) or Power (P$_{max}$= V x I), where R$_{ext}$ is the external resistance. Current densities (I) and power densities were normalized to the exposed surface area of the cathode (10 cm^2). Electrochemical performance of modified cathode was evaluated in dual-chamber MFCs by Linear sweep voltammetry (LSV), electrochemical impedance spectroscopy (EIS) using the electrochemical work station CHI660A system (CH Instruments, Inc.) in three-electrode mode. The cathode was working electrode, while anode and Ag/AgCl served as a counter and reference electrode, respectively.

The LSV was carried out by scanning the potential from zero to OCP of the cathode at the scan rate of 0.1 mV/s. The EIS analysis was performed over a frequency range from 100 kHz to 10 mHz with an AC signal of 10mV amplitude at OCP of the cathode. Electrolyte resistance, polarization /charge transfer resistance (R$_{ct}$), and diffusion resistance (W) were estimated by Nyquist plot. Moreover, electrochemical fitting of impedance spectra was done to the equivalent circuit using the Z view software. However, electrochemical reduction of Cr(VI) on various cathodes were evaluated by cyclic voltammetry using the electrochemical work station CHI660A system (CH Instruments, Inc.) in three-electrode mode, where cathode

was working electrode in the presence of platinum sheet (1 cm x 1 cm) and Ag/AgCl as counter and reference electrode respectively. The potential was scanned from - 1.2 V to + 1.2 V with the scan rate of 10 mV/s. The Cr(VI) concentration in catholyte samples was determined by standard 1,5-diphenyl carbazide-colorimetric method and the UV–vis spectrophotometer (Carry 100, Varian, USA) as described in the literature [3].

Sampling aliquots were collected using the 1 mL syringe and were filtered through 0.45 µm membrane filters before the Cr(VI) determination. Each test was performed thrice, and results are presented as mean value with standard deviation. Equation 1 was used to determine the removal of Cr(VI) efficiency. Cathodic coulombic efficiency (C.E$_{ca}$) represents the ratio of charges used for Cr(VI) reduction to Cr(III) charges flowing across the MFC. Thus C.E$_{ca}$ was calculated by equation.2 as described in previous studies [11]. Where, α is the number of electrons to reduce the Cr(VI), ΔC is the change in concentration during the operation time t, V_{ca} is the volume of cathode chamber, M$_{Cr}$ (52 g/mol) the molecular weight of Cr, F the Faraday's constant (96,485 C/mole), 10^3 the conversion unit (mg/g), I is the circuital current and T is the operation time of MFC. Effect of initial dosage is not only necessary to evaluate the performance of catalytic material but also for implementation of MFC mediated Cr(VI) reduction in real wastewater. Therefore, Cr(VI) reduction efficiency was evaluated with low concentrations. Five MFC-FeS@rGO with various concentrations (i.e, 5, 10, 15, 20, 25, 50 mg/L) and pH 2 were run. MFC performance for Cr(VI) reduction can be influenced by pH of electrolytes. Overall pH change in catholyte can alter the ionic concentration, membrane potential for proton shuttling and Cr(VI) reduction. Therefore, Cr(VI) reduction efficiency was also studied under different pH values. To study the effect of pH, ten parallel MFCs were run with different catholyte pH (1-10) and the same initial concentration (15 mg/L) of Cr(VI).

$$\text{Chromium removal efficiency (\%)} = E_{Rem} = \frac{C_0 - C_t}{C_0} \times 100 \qquad (1)$$

$$C.E_{ca} = \frac{aF \, \Delta C_{cr(IV)} \, V_{Ca}}{10^3 \, M_{Cr \, \sum_{i=1}^{n} li\Delta ti}} \qquad (2)$$

3. Results and discussion

3.1 *FeS@rGO nanocomposite synthesis and characterization*

The synthesis procedure of FeS@rGO nanocomposites is shown in Fig. 1. Graphene oxide (GO) suspension was completely dispersed in $Fe(NO_3)_3$ solution under ultrasonication. Fe^{3+} ions were adsorbed on defects and functional groups (e.g., -OH, -COOH) present on the surface of GO [24]. A black precipitate of FeS was formed when iron nitrate was introduced in the above reaction mixture. Vigorous shaking and ultrasonication ensured the FeS nanoparticles were wrapped in graphene oxide nanosheets [25]. Subsequently, annealing leads to the formation of crystallized FeS wrapped by rGO due to the removal of carboxylic groups and vaporization of intercalated water molecules [26]. The surface morphologies of FeS and FeS@rGO nanocomposites is presented in Fig. 2. The SEM images of FeS and FeS@rGO indicate spherical morphology of nanocomposites (Fig. 2a-b). Moreover, elemental mapping of FeS@rGO nanocomposites confirmed the equal distribution of Fe, S, and C, which depict the wrapping of FeS nanoparticles by rGO nanosheets (Fig. 2c-f). The HR-TEM images also indicate that clear lattice fringes for rGO layers wrapped around the FeS (Fig. 3g-i). Thus, spherical FeS@rGO nanocomposites were prepared with a diameter of 10-35 nm.
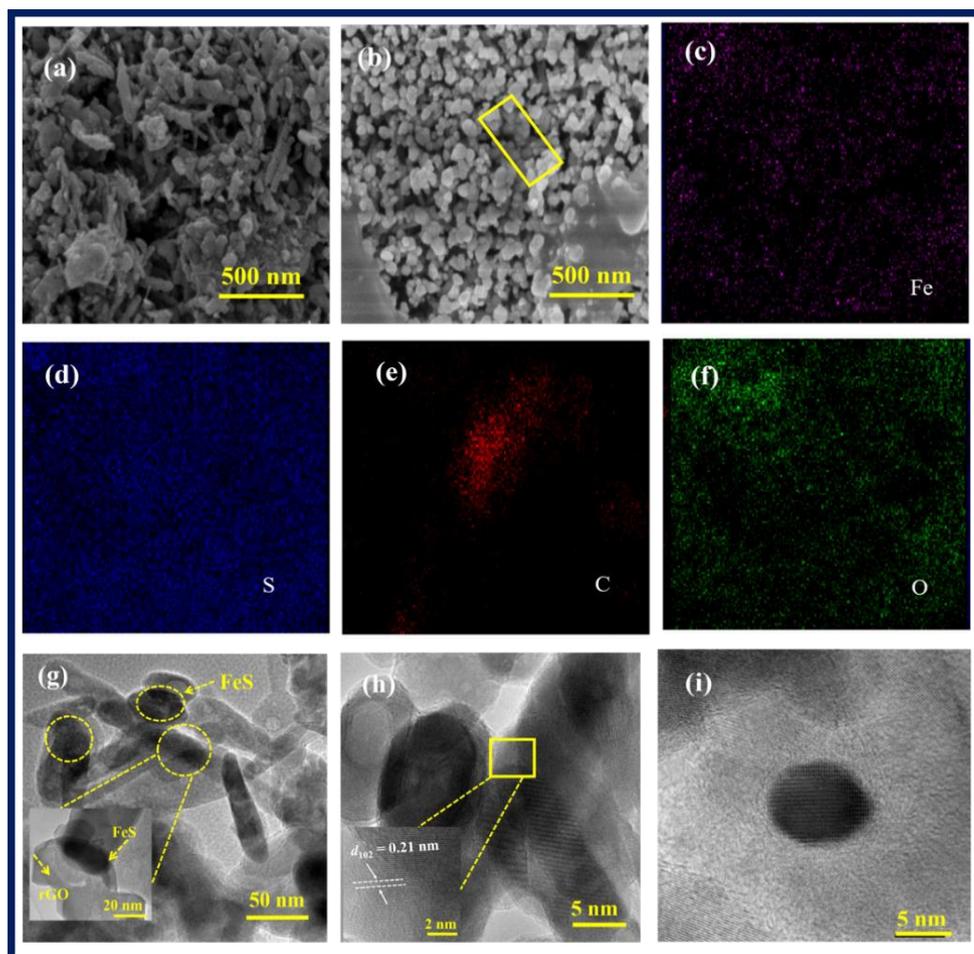
Fig. 2. SEM images of FeS (a) and FeS@rGO (b), elemental mapping of FeS@rGO (c-f), HR-TEM images of Fes@rGO (g-i)

The XRD pattern of synthesised nanocomposite indicated the presence of pure FeS crystals (Fig. 3a). All the diffraction peaks in both samples can be attributed to the FeS (JCPDS 01-075-0600). No iron oxide was detected, which implies that rGO wrapping has prevented the decomposition of FeS to Fe [27]. FTIR spectra of GO showed a short stretching peak of C-O from the carboxyl group at 1725 cm^{-1} (Fig. 3b). The broad hydroxyl stretching peak was observed at 3200 cm^{-1}. The intense peaks around 1635 cm^{-1}, 1420 cm^{-1} and 1060 cm^{-1} represent the C-C vibration of aromatic hydrocarbons (SP2 characteristic of graphene), C-O (carboxy) and alkoxy peaks of graphene oxide respectively (Fig. 3b). Intriguingly, hydroxyl peak shift toward higher wavenumber and complete disappearance of peak 1725 cm^{-1} for FeS@rGO indicate the removal of oxygen-containing function groups from GO [28]. Also, a short peak representing the aromatic C=O of at 1625 cm^{-1} indicates the reduction of GO after pyrolysis. A clear shift at peaks 1109 and 1153 in FeS@rGO spectra may be assigned to steric hindrance after combining the rGO with FeS nanoparticles [29].

XPS analysis was used to characterize the chemical states of FeS@rGO composites. XPS survey spectra of nanocomposites confirmed the presence of Fe, S, and C (Fig. 3c). Binding energies of 708.7 eV and 722.4 eV for Fe 2p$_{3/2}$ and Fe 2p$_{1/2}$ can be ascribed to Fe^{2+} state in Fe 2p spectrum of FeS@rGO respectively (Fig. 3d). In S 2p spectra of FeS@rGO the core level band of the S 2p area can be spotted with the peaks around 160.5 eV and 162 eV corresponding to the S 2p$_{1/2}$ and S 2p$_{3/2}$ as a characteristic of FeS (Fig. 3e). The C 1s features of GO in XPS spectra showed the peaks compatible to the sp2 bonded carbon (C-C) and carboxylic/carbonyl (C=O) components at 283.8, 286 and 287.9 eV respectively (Fig. 3f). The relatively intense peak of C-C compared with C-O and C=O showed the reduction of GO after annealing step [25, 30]. XPS results reinforced the findings of XRD and TEM. Overall characterization revealed that FeS@rGO nanocomposites were successfully synthesized for the application of chromate reduction.
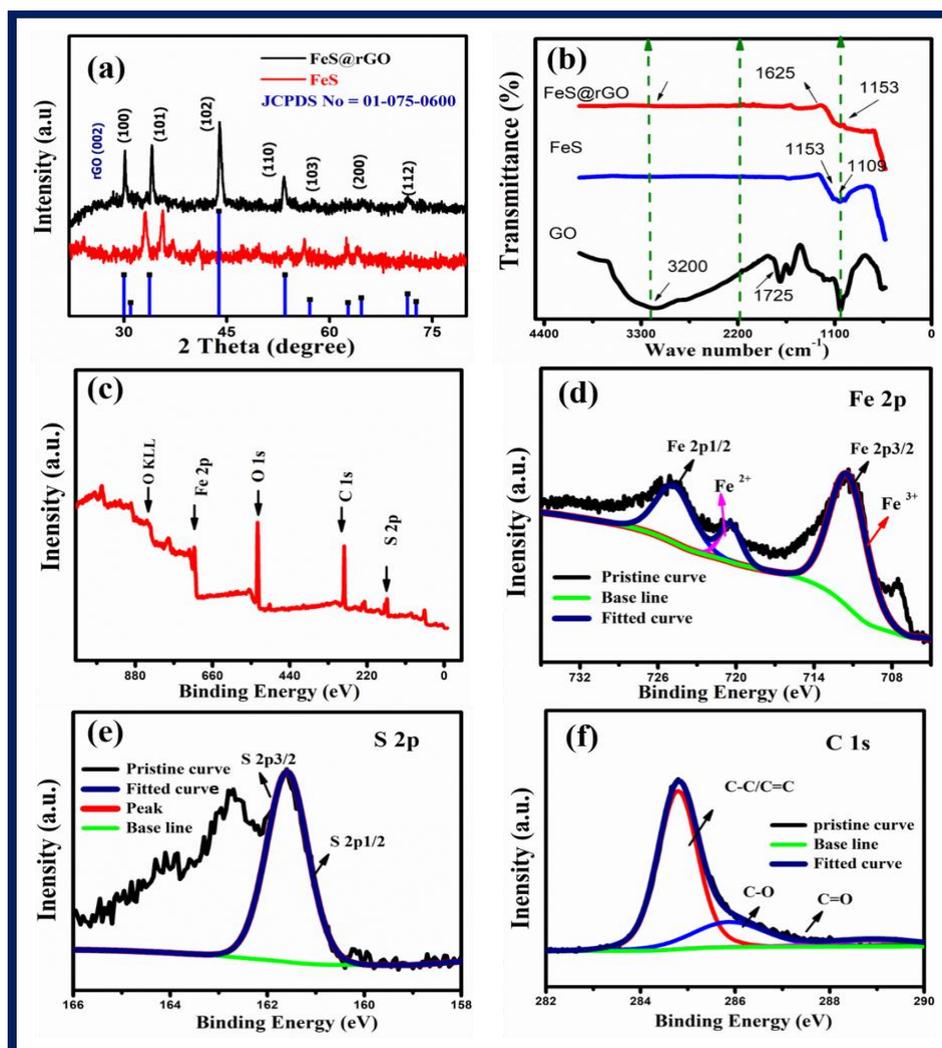
Fig. 3. XRD spectra of FeS and FeS@rGO (a), FITR Spectra (b), XPS spectra of FeS@rGO, survey spectrum(c), Fe 2p (d), S 2p (e), C 1s(f)

3.2 Electrochemical performance of FeS@rGO decorated electrode.

Electrochemical reduction of Cr(VI) using modified electrodes in MFC was investigated by CV method using the three-electrode system, where cathode was working electrode in the presence of Ag/AgCl reference electrode and Pt as a counter electrode. Distal water was filled in FeS@rGO containing MFC as a negative control. Cyclic voltammogram from all MFCs showed reduction peaks except negative control (Fig. 4a). The reduction peak from MFC-blank was weak (-0.82 V), which indicate the slow reduction of Cr(VI) at the surface of the unmodified cathode. Graphite felt modified with FeS@rGO exhibited the wide reduction peak at - 0.17 V (vs Ag/AgCl) and high catalytic current (I = - 7.7 e^{-3} A) compared with MFC-FeS which displayed the lower reduction peaks around the -0.54 V and catalytic current of -3.2 e^{-2} A (Fig. 4a). Previous studies have evinced the Cr(VI) reduction within the

range of 0.6 V to -0.8 V. A positive shift in the reduction peak for MFC-FeS@rGO depict the low overpotential and enhanced electrocatalytic reduction of Cr(VI). Similar positive shifts for Cr(VI) reduction potential have been observed after electrode modification with efficient catalytic materials [10, 31]. Enhanced electrocatalytic performance of MFC-FeS@rGO compared with controls can be attributed to the FeS@rGO nanocomposites, which signify that rGO in FeS@rGO have improved electron transfer kinetics due to excellent conductivity and large surface area.

The LSV analysis also confirmed the electrocatalytic reduction of Cr(VI), and the resulting current was highest for MFC-FeS@rGO compared with controls (Fig. 4b). The high current generation can be linked with a high flux of Cr(VI) species on the surface of FeS@rGO containing cathode [3]. Thus, fast Cr(VI) reduction will be achieved for modified cathode by FeS@rGO nanocomposites. Further electrochemical performance of modified electrodes was evaluated by EIS analysis. The EIS analysis is useful to measure the internal resistance or reasons for voltage losses for various electrodes. Generally, internal resistance comprised of ohmic resistance (R_{ohm}), Charge transfer resistance (R_{ct}) and Warburg/diffusional resistance (W) of the electrode. One-time constant model (OTCM) was selected to calculate all above parameters of EIS. The Nyquist plots and equivalent circuit diagram are shown in Fig. 4c. The ohmic resistance and charge transfer resistance are estimated from the diameter of first and second intercept, respectively at the real impedance axis [32]. The ohmic resistance for MFC-FeS@rGO (3.12 Ω) was slightly lower than the MFC-FeS (4.26 Ω) and MFC-blank (4.9 Ω) (Table 1 & Fig. 4c). The low ohmic resistance of electrolyte is effective for superior conductivity and accelerated electron mobility [23].

Lowest R_{ct} for MFC-FeS@rGO (2.86 Ω) compared with MFC-FeS (6.15 Ω) and MFC-blank (11.26 Ω) can be ascribed to the evident conductivity due to FeS@rGO nanocomposites attached on graphite felt. Moreover, FeS@rGO nanocomposite network has provided more electroactive surface area to improve the electron transfer by reducing the interfacial contact resistance between cathode and catholyte [33]. Charge transfer resistance is referred to as the activation energy of cathode; therefore, a better Cr(VI) reduction kinetics for MFC-FeS@rGO are observed. Similarly, diffusional resistance (W) was also reduced in modified cathodes, which implies that FeS@rGO combination was useful for low activation energy, enhanced Cr(VI) reduction and overall better performance of MFC (Fig. 4c). These findings are consistent with the CV, LSV results, and reduction efficiencies, which have demonstrated that FeS@rGO nanocomposites as a potential cathode modifier for simultaneous Cr(VI) reduction

11

and electricity generation. The maximum output performance of MFCs was analysed by polarization curves obtained by varying the external resistance method.

The maximum power density of MFC-FeS@rGO was 90.4 mW/m^2, which was 60% and 150% higher as that of MFC-FeS (56 mW/m^2) and MFC-blank (36 mW/m^2) respectively (Fig. 4d). The results indicated that the electrodes modified with FeS@rGO nanocomposites had exhibited the favourable electrochemical performance; thus, they can be used as a potential modifier for cathodes. Similarly, maximum extracted current density from MFC-FeS@rGO (488mA/m^2) was 84% and 140 % higher than MFC-FeS (264 mA/m^2) and MFC-blank (200 mA/m^2) respectively (Fig. 4d). The improved electrochemical performance of FeS@rGO can be linked with low internal resistance and efficient charge transfer ability of rGO [29]. Noticeably, the maximum power density extracted in this study was higher than the previous studies used for simultaneous electricity generation and Cr(VI) reduction from concentrated wastewater [3, 34, 35]. Briefly, our electrode has demonstrated a better performance compared with previous studies in terms of high reduction peak and catalytic current and internal resistance [3, 10, 31] .
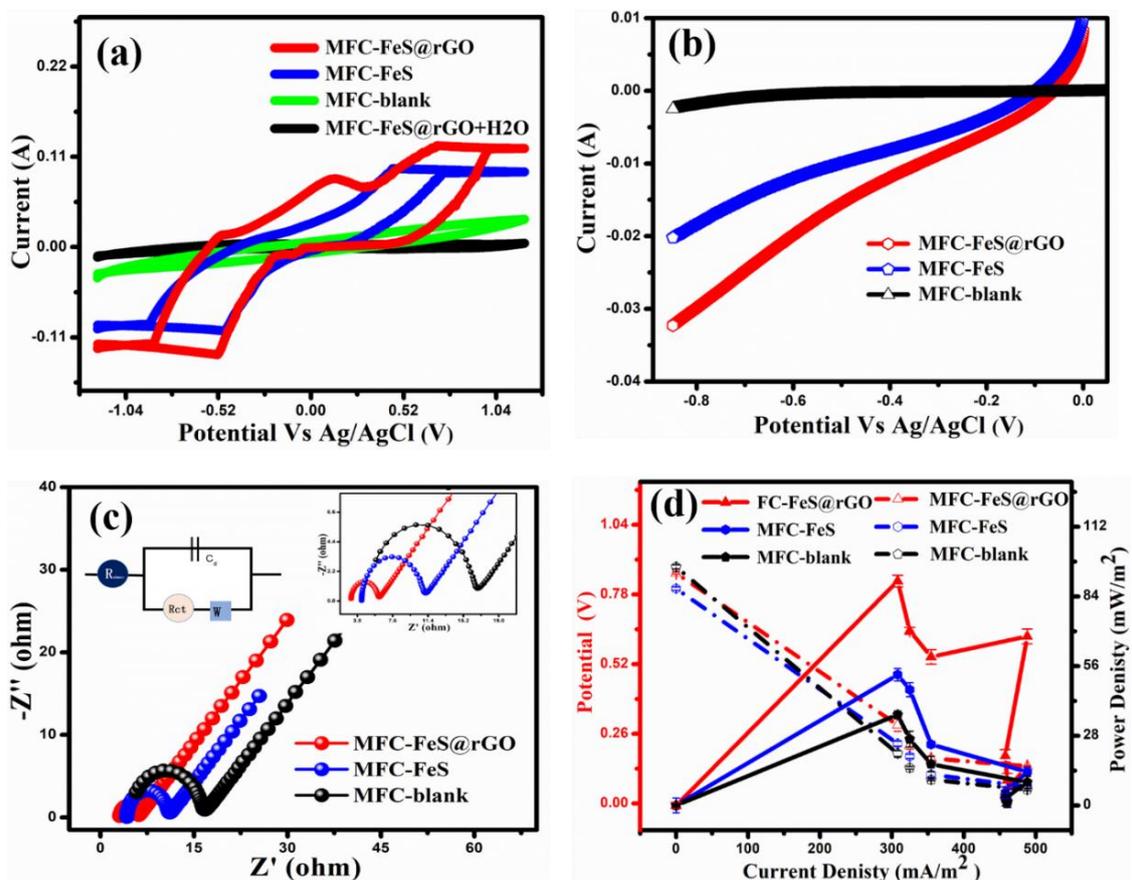
Fig. 4. Cyclic voltammetry (a), Linear sweep voltammetry (b), Electrochemical impendence spectroscopy (c), Polarization curves (d)

Table. 1 Detailed parameters and components of EIS

MFC	R_{ohm} (Ω)	RCT (Ω)	Warburg	Capacitance
MFC-FeS@rGO	3.12	2.86	0.0117	1.10E-05
MFC-FeS	4.26	6.515	0.1922	4.80E-05
MFC-blank	4.916	11.26	0.01862	6.02E-07

3.3 Cr(VI) reduction performance of MFC

Electrochemical Cr(VI) reduction performance of MFCs was evaluated using the different modified electrodes. Three MFCs, having different cathodes, were filled with 15 mg/L of Cr(VI). The MFC-FeS@rGO exhibited a rapid reduction in the Cr(VI) concentration and 100% removal after 10.5 h (Fig. 5a). Meanwhile, Cr(VI) removal efficiency was 57% and 81% for MFC-FeS and MFC-blank, respectively. Remarkably, FeS@rGO nanocomposites have accelerated the Cr(VI) reduction in MFC (Fig. 5a). Reduction kinetics of Cr(VI) provided a detailed insight of improved MFC performance, which indicated the complete reduction of Cr(VI) required additional time in control MFCs (Fig. 5b). Cr(VI) reduction data was approximately fitted to the first order of reaction with R^2 = 0.95. The rate constant was calculated from the slope of ln C_0/C vs. time graph, where C_0 and C are initial concentration and concentration at time t (Fig. 5b). Enhanced reduction kinetics for MFC-FeS@rGO was also apparent from the reduction rate. The reduction rate for MFC-FeS@rGO (1.43 mg/L/h) was approximately 2.0 and 4.6 times higher than MFC-FeS and MFC-blank, respectively.

Interestingly, the Cr(VI) reduction rate in this study was highest among the previously reported studies using a high concentration of catholytes [10, 36-38]. Accelerated reduction from Cr(VI) to Cr(III) can also be linked with the enhanced electrogenic activity of anodic microbes [34]. Relatively, a stabilized and high current density was generated from MFC-FeS@rGO compared with control MFCs (Fig. 5c). Cathodic coulombic efficiency (*C.E$_{ca}$*) depicted the number of electrons consumed for Cr(VI) reduction. MFC-FeS@rGO exhibited the highest *C.E$_{ca}$* (61%) compared with MFC-FeS (31%) and MFC-blank (17%), respectively (Fig. 5d). Therefore, an adequate number of electrons were produced and transferred to the

cathodes as a result of superior reaction kinetics in MFC-FeS@rGO. The favourable electrochemical reaction kinetics at the cathode and better electrogenic activity, in turn, affect the consumption of anodic substrate [39]. Therefore COD removal efficiency of all MFCs was also analysed along with Cr(VI) reduction. MFC-FeS@rGO revealed the highest COD removal efficiency (72%) compared with MFC-FeS (48%) and MFC-blank (23%) respectively control MFCs (Fig. 5d). Frequent replenishment of annolyte will substantially improve the wastewater treatment efficiency of MFCs. It implies that cathode modification with efficient catalysts does not only accelerate the Cr(VI) reduction but also improve the electrogenic activity which may lead to the enhanced consumption of anodic substrate and high power generation from wastewater.
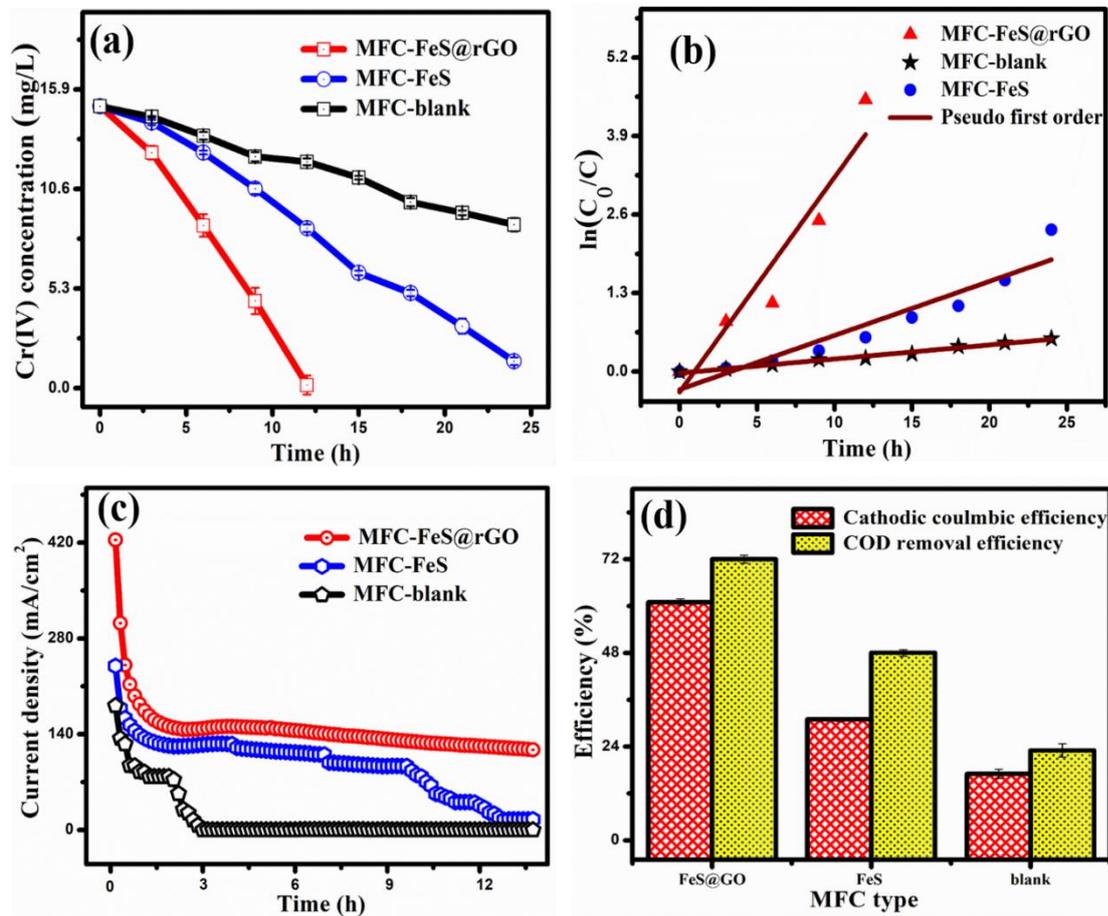
Fig. 5.

Cr (IV) reduction profile (a), Reaction kinetics (b), Current density profile(c), Cathodic coulombic and COD removal efficiency (d)

3.4 Effect of initial concentration and pH on Cr(VI) reduction performance

14

Effect of initial Cr(VI) concentrations on the reduction and catalytic performance of MFCs was also evaluated here. Reduction efficiency was increased with the initial concentration of Cr(VI) up to 15 mg/L. However, later on, reduction efficiency was decreased (Fig. 6a). Results indicated that 15 mg/L concentration has delivered the highest Cr(IV) removal efficiency (99.9 %). The decrease in Cr(VI) reduction efficiency at high concentration can be specified with a high number of electron acceptors compared with electrons produced through metabolism [31]. Negative impacts of high concentration on Cr(VI) reduction efficiency and MFC performance have already been reported [40]. In literature, usually, a high concentration (100-300 mg/L) of Cr(VI) is used to show the high power production and removal efficiency in MFC [41-43]. This high concentration of Cr(VI) is unrealistic and is far from real wastewater. Therefore, Cr(VI) reduction efficiency at low concentration is necessary to investigate and to apply this lucrative technology for real wastewater.

Furthermore, effect of different pH values on reduction efficiencies was studied to explore further insights of reaction kinetics. Fig. 6b revealed that complete Cr(VI) reduction was achieved for pH two after 10.5 h. For other pH values, the removal efficiency was lower and would require more reaction time for complete reduction. Generally, the reduction rate was increased with the decrease of pH 2-10. Under acidic conditions, Cr(VI) reduction is thermodynamically favourable due to increase in standard reduction potential by hydrogen ions [44]. However, the reduction rate was not further increased for pH 1, which can be ascribed to the hydrogen ions movement from cathode to anode to shatter the essential pH gradient for microbial growth. So current study has showed the high Cr(VI) reduction efficiency for low concentrated wastewater, thus it aims to fill the gaps for practical applications of MFC mediated Cr(VI) reduction.
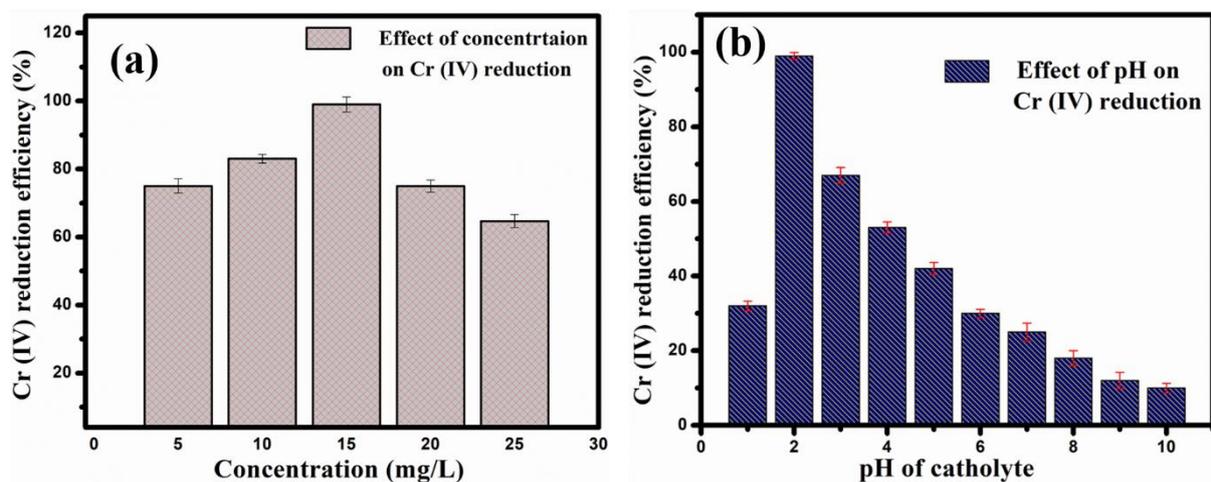
Fig. 6. Effect of the initial concentration of Cr (VI) (a), Effect of pH on the reduction efficiency of Cr (VI) (b).

4. Conclusion

In this study, FeS@rGO nanocomposites synthesized by facile precipitation method were used to decorate the graphite felt cathode. The modified cathode in dual-chamber MFC was found to be superior for synergistic Cr(VI) reduction and electricity generation. Electrochemical characterisation revealed the enhanced performance was due to excellent conductivity, low internal resistance, and improved electrochemical performance of FeS@rGO. Detailed reduction kinetics depicted that rapid Cr(VI) reduction has positive influence on the COD removal efficiency and electrogenic activity in the anode. High power production and cathodic coulombic efficiency evinced the significant charge consumption was due to Cr(VI) reduction. Overall our findings suggest this method has potential implications for scaling up MFC technology in real wastewater treatment. Thus, despite the high Cr(VI) removal efficiency in lab experiment, further studies are needed to evaluate this material for real wastewater.

Conflicts of Interest: The authors declare no conflict of interests.

References

[1] Y. Li, Y. Bian, H. Qin, Y. Zhang, Z. Bian, Photocatalytic reduction behavior of hexavalent chromium on hydroxyl modified titanium dioxide, Applied Catalysis B: Environmental, 206 (2017) 293-299.
[2] Y. Xie, S. Holmgren, D.M. Andrews, M.S. Wolfe, Evaluating the impact of the US National toxicology program: A case study on hexavalent chromium, Environmental health perspectives, 125 (2017) 181.

[3] M. Li, S. Zhou, Y. Xu, Z. Liu, F. Ma, L. Zhi, X. Zhou, Simultaneous Cr (VI) reduction and bioelectricity generation in a dual chamber microbial fuel cell, Chemical Engineering Journal, 334 (2018) 1621-1629.

[4] R.N. Bharagava, S. Mishra, Hexavalent chromium reduction potential of Cellulosimicrobium sp. isolated from common effluent treatment plant of tannery industries, Ecotoxicology and environmental safety, 147 (2018) 102-109.

[5] D.M. Hausladen, A. Alexander-Ozinskas, C. McClain, S. Fendorf, Hexavalent Chromium Sources and Distribution in California Groundwater, Environmental science & technology, 52 (2018) 8242-8251.

[6] Q. Cheng, C. Wang, K. Doudrick, C.K. Chan, Hexavalent chromium removal using metal oxide photocatalysts, Applied Catalysis B: Environmental, 176 (2015) 740-748.

[7] J. Huang, Y. Cao, Q. Shao, X. Peng, Z. Guo, Magnetic nanocarbon adsorbents with enhanced hexavalent chromium removal: morphology dependence of fibrillar vs particulate structures, Industrial & Engineering Chemistry Research, 56 (2017) 10689-10701.

[8] Z. Wang, M. Murugananthan, Y. Zhang, Graphitic carbon nitride based photocatalysis for redox conversion of arsenic (III) and chromium (VI) in acid aqueous solution, Applied Catalysis B: Environmental, 248 (2019) 349-356.

[9] J. Ali, A. Sohail, L. Wang, M. Rizwan Haider, S. Mulk, G. Pan, Electro-microbiology as a promising approach towards renewable energy and environmental sustainability, Energies, 11 (2018) 1822.

[10] M. Li, S. Zhou, α-Fe2O3/polyaniline nanocomposites as an effective catalyst for improving the electrochemical performance of microbial fuel cell, Chemical Engineering Journal, 339 (2018) 539-546.

[11] Q. Wang, L. Huang, Y. Pan, X. Quan, G.L. Puma, Impact of Fe (III) as an effective electron-shuttle mediator for enhanced Cr (VI) reduction in microbial fuel cells: Reduction of diffusional resistances and cathode overpotentials, Journal of hazardous materials, 321 (2017) 896-906.

[12] T.-s. Song, Y. Jin, J. Bao, D. Kang, J. Xie, Graphene/biofilm composites for enhancement of hexavalent chromium reduction and electricity production in a biocathode microbial fuel cell, Journal of hazardous materials, 317 (2016) 73-80.

[13] S.A. Baig, Q. Wang, Z. Wang, J. Zhu, Z. Lou, T. Sheng, X. Xu, Hexavalent chromium removal from solutions: surface efficacy and characterizations of three iron containing minerals, CLEAN–Soil, Air, Water, 42 (2014) 1409-1414.

[14] M. Park, J. Park, J. Kang, Y.-S. Han, H.Y. Jeong, Removal of hexavalent chromium using mackinawite (FeS)-coated sand, Journal of hazardous materials, 360 (2018) 17-23.

[15] A. Ashraf, I. Bibi, N.K. Niazi, Y.S. Ok, G. Murtaza, M. Shahid, A. Kunhikrishnan, D. Li, T. Mahmood, Chromium (VI) sorption efficiency of acid-activated banana peel over organo-montmorillonite in aqueous solutions, International journal of phytoremediation, 19 (2017) 605-613.

[16] J. Shi, W. Zhao, C. Liu, T. Jiang, H. Ding, Enhanced Performance for Treatment of Cr (VI)-Containing Wastewater by Microbial Fuel Cells with Natural Pyrrhotite-Coated Cathode, Water, 9 (2017) 979.

[17] I. Ivanov, Y. Ahn, T. Poirson, M.A. Hickner, B.E. Logan, Comparison of cathode catalyst binders for the hydrogen evolution reaction in microbial electrolysis cells, international journal of hydrogen energy, 42 (2017) 15739-15744.

[18] L. Fei, Q. Lin, B. Yuan, G. Chen, P. Xie, Y. Li, Y. Xu, S. Deng, S. Smirnov, H. Luo, Reduced graphene oxide wrapped FeS nanocomposite for lithium-ion battery anode with improved performance, ACS applied materials & interfaces, 5 (2013) 5330-5335.

[19] H. Xue, Y. Denis, J. Qing, X. Yang, J. Xu, Z. Li, M. Sun, W. Kang, Y. Tang, C.-S. Lee, Pyrite FeS 2 microspheres wrapped by reduced graphene oxide as high-performance lithium-ion battery anodes, Journal of Materials Chemistry A, 3 (2015) 7945-7949.

[20] X. Jiang, J. Hu, A.M. Lieber, C.S. Jackan, J.C. Biffinger, L.A. Fitzgerald, B.R. Ringeisen, C.M. Lieber, Nanoparticle facilitated extracellular electron transfer in microbial fuel cells, Nano letters, 14 (2014) 6737-6742.

[21] W. Yang, G. Chata, Y. Zhang, Y. Peng, J.E. Lu, N. Wang, R. Mercado, J. Li, S. Chen, Graphene oxide-supported zinc cobalt oxides as effective cathode catalysts for microbial fuel cell: High catalytic activity and inhibition of biofilm formation, Nano Energy, 57 (2019) 811-819.

[22] X. Wang, S. Cheng, Y. Feng, M.D. Merrill, T. Saito, B.E. Logan, Use of carbon mesh anodes and the effect of different pretreatment methods on power production in microbial fuel cells, Environmental science & technology, 43 (2009) 6870-6874.

[23] J. Ali, L. Wang, H. Waseem, H.M.A. Sharif, R. Djellabi, C. Zhang, G. Pan, Bioelectrochemical recovery of silver from wastewater with sustainable power generation and its reuse for biofouling mitigation, Journal of Cleaner Production, 235 (2019) 1425e1437.

[24] R. Sitko, E. Turek, B. Zawisza, E. Malicka, E. Talik, J. Heimann, A. Gagor, B. Feist, R. Wrzalik, Adsorption of divalent metal ions from aqueous solutions using graphene oxide, Dalton transactions, 42 (2013) 5682-5689.

[25] S.Y. Lee, Y.C. Kang, Sodium‐Ion Storage Properties of FeS–Reduced Graphene Oxide Composite Powder with a Crumpled Structure, Chemistry–A European Journal, 22 (2016) 2769-2774.

[26] J.D. Renteria, S. Ramirez, H. Malekpour, B. Alonso, A. Centeno, A. Zurutuza, A.I. Cocemasov, D.L. Nika, A.A. Balandin, Strongly anisotropic thermal conductivity of free‐standing reduced graphene oxide films annealed at high temperature, Advanced Functional Materials, 25 (2015) 4664-4672.

[27] X. Wen, X. Wei, L. Yang, P.K. Shen, Self-assembled FeS 2 cubes anchored on reduced graphene oxide as an anode material for lithium ion batteries, Journal of Materials Chemistry A, 3 (2015) 2090-2096.

[28] A.M. Golsheikh, N. Huang, H. Lim, C.H. Chia, I. Harrison, M. Muhamad, One-pot hydrothermal synthesis and characterization of FeS2 (pyrite)/graphene nanocomposite, Chemical engineering journal, 218 (2013) 276-284.

[29] W. Chen, S. Qi, L. Guan, C. Liu, S. Cui, C. Shen, L. Mi, Pyrite FeS 2 microspheres anchoring on reduced graphene oxide aerogel as an enhanced electrode material for sodium-ion batteries, Journal of Materials Chemistry A, 5 (2017) 5332-5341.

[30] S.H. Aboutalebi, A.T. Chidembo, M. Salari, K. Konstantinov, D. Wexler, H.K. Liu, S.X. Dou, Comparison of GO, GO/MWCNTs composite and MWCNTs as potential electrode materials for supercapacitors, Energy & Environmental Science, 4 (2011) 1855-1865.

[31] S. Gupta, A. Yadav, N. Verma, Simultaneous Cr (VI) reduction and bioelectricity generation using microbial fuel cell based on alumina-nickel nanoparticles-dispersed carbon nanofiber electrode, Chemical Engineering Journal, 307 (2017) 729-738.

[32] F. Ndayisenga, Y. Yu, C.-H. Lay, D. Zhou, Bioelectricity generation using microalgal biomass as electron donor in a bio-anode microbial fuel cell, Bioresource Technology, (2018).

[33] M. Sindhuja, S. Harinipriya, A.C. Bala, A.K. Ray, Environmentally available biowastes as substrate in microbial fuel cell for efficient chromium reduction, Journal of hazardous materials, 355 (2018) 197-205.

[34] L. Huang, X. Chai, G. Chen, B.E. Logan, Effect of set potential on hexavalent chromium reduction and electricity generation from biocathode microbial fuel cells, Environmental science & technology, 45 (2011) 5025-5031.

[35] L. Liu, Y. Yuan, F.-b. Li, C.-h. Feng, In-situ Cr (VI) reduction with electrogenerated hydrogen peroxide driven by iron-reducing bacteria, Bioresource technology, 102 (2011) 2468-2473.

[36] Y. Li, A. Lu, H. Ding, S. Jin, Y. Yan, C. Wang, C. Zen, X. Wang, Cr (VI) reduction at rutile-catalyzed cathode in microbial fuel cells, Electrochemistry Communications, 11 (2009) 1496-1499.

[37] Y. Pang, D. Xie, B. Wu, Z. Lv, X. Zeng, C. Wei, C. Feng, Conductive polymer-mediated Cr (VI) reduction in a dual-chamber microbial fuel cell under neutral conditions, Synthetic Metals, 183 (2013) 57-62.

[38] L. Huang, Q. Wang, L. Jiang, P. Zhou, X. Quan, B.E. Logan, Adaptively evolving bacterial communities for complete and selective reduction of Cr (VI), Cu (II), and Cd (II) in biocathode bioelectrochemical systems, Environmental science & technology, 49 (2015) 9914-9924.

[39] J.S. Sravan, S.K. Butti, A. Verma, S.V. Mohan, Phasic availability of terminal electron acceptor on oxygen reduction reaction in microbial fuel cell, Bioresource technology, 242 (2017) 101-108.

[40] W. Xu, H. Zhang, G. Li, Z. Wu, A urine/Cr (VI) fuel cell—electrical power from processing heavy metal and human urine, Journal of Electroanalytical Chemistry, 764 (2016) 38-44.

[41] M. Tandukar, S.J. Huber, T. Onodera, S.G. Pavlostathis, Biological chromium (VI) reduction in the cathode of a microbial fuel cell, Environmental science & technology, 43 (2009) 8159-8165.

[42] N. Habibul, Y. Hu, Y.-K. Wang, W. Chen, H.-Q. Yu, G.-P. Sheng, Bioelectrochemical chromium (VI) removal in plant-microbial fuel cells, Environmental science & technology, 50 (2016) 3882-3889.

[43] B. Zhang, C. Feng, J. Ni, J. Zhang, W. Huang, Simultaneous reduction of vanadium (V) and chromium (VI) with enhanced energy recovery based on microbial fuel cell technology, Journal of Power Sources, 204 (2012) 34-39.

[44] F. Rodriguez-Valadez, C. Ortiz-Éxiga, J.G. Ibanez, A. Alatorre-Ordaz, S. Gutierrez-Granados, Electroreduction of Cr (VI) to Cr (III) on reticulated vitreous carbon electrodes in a parallel-plate reactor with recirculation, Environmental science & technology, 39 (2005) 1875-1879.